Research Article / Review Article FUPRE JOURNAL 7(3):108-121 (2023)

FUPRE Journal

of

Scientific and Industrial Research

ISSN: 2579-1184(Print) ISSN: 2578-1129 (Online)

http://fupre.edu.ng/journal

Application of Numerical and Computational Based Models for Modelling the Effects of the Electrode Density in Mild Steel TIG Welding Process

AMADHE, F. O.[1,*], **[1]ACHEBO, J. I.**[1], **OBAHIAGBON, K.**[2], **OZIGAGUN, A.**[1,*]

[1]*Department of Production Engineering, University of Benin, Benin City, Nigeria*

[2]*Department of Chemical Engineering, University of Benin, Benin City, Nigeria*

ARTICLE INFO

Received: 12/04/2023
Accepted: 01/06/2023

Keywords

Artificial Neural Network, Electrode density, Mild Steel, Response surface methodology, Tungsten Inert Gas welding

ABSTRACT

The well-known arc welding technique of Tungsten Inert Gas (TIG) welding is widely used to join thin pieces of practically all ferrous and non-ferrous materials. However, there have been many improvements made to the TIG welding process as a result of the increased interest of industries in using the method for joining components with mid-thick sections. In the study, emphasis was placed on the density of the TIG electrode being welded with mild steel in which the studies employed 100 pieces of coupons made of mild steel that were 80 x 40 x 10 (mm) in size. Using 5 specimens each time, the experiment was done 20 times. The plates' edges were machined and bevelled before being welded using tungsten inert gas welding equipment. The Response Surface Methodology (RSM) and the Artificial Neural Network (ANN) were used to ascertain and optimize the electrode density of the welded specimen. The RSM model generated a numerically ideal solution with the following values: 200.72A current, 20V voltage, 2.40mm wire diameter, and 20m/s wire feed speed, resulting in an electrode density of 6511.24kgm/s2. With a desirability value of 93.9%, the design expert determined that this solution was the best option. In the ANN, 70% of the data was used for training, 15 % was used for validating and the last 15% for the actual test. From the results obtained a regression plot that displays the relationship between the input factors and the desired outcome was produced with R2 values of 0.84831. The ANN is selected as the better predictive model over the RSM because the ANN output fits closer to the experimental than that of RSM. Thus, the approaches effectively optimized and predicted the electrode density.

1. INTRODUCTION

High corrosion resistance, weldability, long service life, formability, and non-magnetic characteristics are all attributes of the alloy known as stainless steel (SS) (Sunilkumar, D. et. al., 2020). Aerospace, automotive, construction, rolling, chemical processing, household products, and other industries use stainless steel extensively (Hall, J. N. and Fekete, J. R., 2017) (Bhadeshia, H. and Honeycombe, R., 2017). Thin portions of mild and stainless steel are frequently joined using the Gas Tungsten Arc Welding (GTAW) or Tungsten Inert Gas (TIG) procedures (Dipali P. et. al., 2021). Figure

*Corresponding author, e-mail:author@fupre.edu.ng
DIO

1A illustrates a TIG welding process while Figure 1B

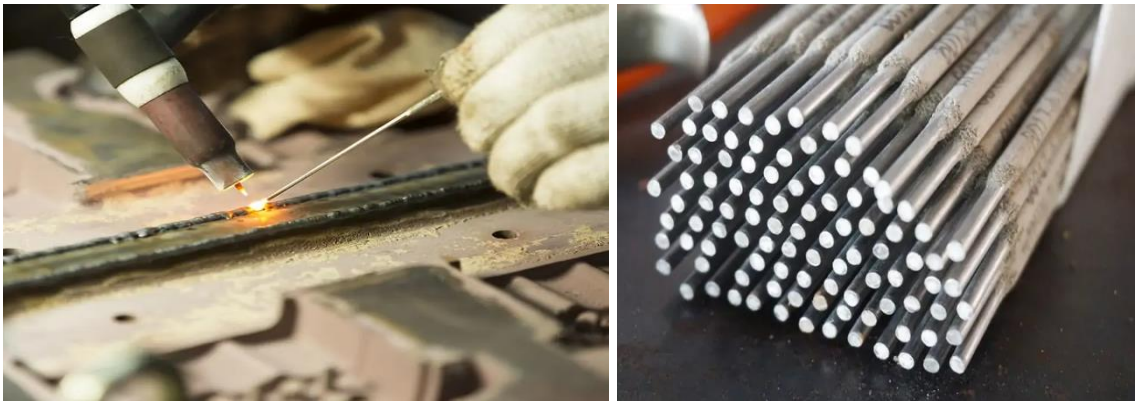

Figure 1: (A) TIG welding process (Aumm graphixphoto) (B) TIG electrodes (Pongsak14)

A series of research papers analyzed the behavior of TIG processes have been studied for several decades. The earliest investigations looked at the haphazard relationships between the input factors, the electrode fusion rate, and the metal (Meneses, L. et. al., 2019). It is well known among TIG welders that spatter reduces the quality of welded joints, thus attracting further finishing processes on the product and additional costs for its removal. Sathish T. (2021) reported that tungsten inert gas welding was used to join wrought aluminum AA8006 for industrial purposes. The regression equation was then solved using the multi-objective algorithm while the mechanical and microstructure parameters were being examined. Sarkar P. and Kakoty S. (2021) analyzed the surface toughness, standing tensile strength, and impact loading while taking into account the welding speed, base current, and peak current as process parameters. According to Azadi M. and Kolahan F. (2020), the generated model is useful for modeling and optimizing A-TIG welding. To optimize the parameters, an orthogonal array Taguchi, a regression model, and a variance analysis were used. The flus have been activated using SiO2 nanoparticles. Ragavendran M. et. al. (2017) looked into how using a hybrid laser and TIG welding process affected the response. The welding procedure was carried out using austenitic stainless steel 316LN. Using response surface approach, the effect had been examined for weld bead width, weld cross-sectional area, and penetration depth. The measured and anticipated values show a strong agreement as well. Using the response surface methodology (RSM), Vidyarthy R. (2018) examined the connection between the reaction and the A-TIG welding process parameters, such as welding current, welding speed, and flux coating density. It was found that the welding current has the biggest impact on the weld bead shape. In the course of the A-TIG welding process, Vasantharaja P. and Vasudevan M. (2018) used response surface approach to identify the ideal values. The best values for the welding parameters were found using numerical and graphical optimization. Pamnani R. (2017) conducted tests on DMR249A steel used in ships and aircraft. The RSM methodology and trial design made it possible for this strategy to obtain a good depth of penetration. Singh P. (2017) investigated how the vibratory welding method influenced mild steel plating used to create butt welds. In this

work, the microstructure and micro hardness were also investigated. It was discovered that the vibratory condition increased the hardness value relative to the traditional procedure. Magudeeswaran G. (2014) described how A-TIG was used to determine the ideal aspect ratio for DSS joints. The ANOVA and pooled ANOVA procedures were used to determine the important experimental parameters. The researchers came to the conclusion that the ANOVA analysis revealed that the optimized parameters were within the allowable range. Sivachidambaram P. and Balachandar K. (2015) looked into an approach to welding aluminum and aluminum composite employing optimum pulsed current TIG settings, welding regression equations, and also built an empirical model to determine the key parameters. In this work, the effects of the electrode density parameters were determined while voltage, welding current and gas flow rate were taken into consideration as process parameters. The design of experiment (DOE) methodology was used to create the orthogonal array for the central composite design, which the RSM and ANN then examined.

2.0 METHODS

2.1 Experimental setup

For the experiments, 100 mild steel coupons with measurements of 80 x 40 x 10 (mm) were utilized. The experiment was conducted 20 times, with 5 specimens per run. The plates' edges were machined and bevelled before being welded using tungsten inert gas welding equipment. Mild steel plates of 10 mm thickness were TIG welded using different ranges of current, voltage, wire diameter and wire feed rate. In this investigation, 100% pure Argon gas was employed as a shielding gas throughout the welding process to protect the weld specimen from air interaction. The silicon carbide abrasive sheets were ground using a rotating disk at five stages of 80, 300, 600, 1200, and 4000 grits on all welded samples after they had been cut perpendicular to the welding direction and mounted in resin (Mecatech 334). Following polishing with 3 m (microns) and 1 m (microns) diamond pastes, the specimens were etched by immersing them in sodium hydroxide solution (1g NaOH + 100 ml H2O) as an etchant for 45 seconds. Using an electronic microscope, model number KEYNCE VHX-500F, the samples' macrostructure and microstructure were investigated. Mild steel plate with a 10 mm thickness was used for the weld sample construction. The plate was powered hacksaw cut to size. With the seams welded and the edges ground and polished with emery paper, the electrode density as a response was then measured and recorded. To take consecutive shots of the spatter images from a distance of 0.7 meters, a mobile phone camera was installed and placed above and to the side of the welding region. Spatter shots taken in both the vertical and horizontal directions were combined to create two-dimensional spatter images. Spatter distribution is assessed using shots taken vertically, whereas spatter counting is carried out using photos taken horizontally. At 240 fps, scatter pictures were captured. Due to the welding arc's brilliance, the spatter photos that were collected were primarily distorted. As a result, welding spatter was only tracked using an optical filter. A neutral-density (ND) optical filter was installed on the digital lens, which results in sharper images by evenly dispersing incident light across the wavelength spectrum.

2.2 Design of experiment

A design of experiment is a scientific approach to organizing and carrying out an experiment that will reveal a cause-and-

effect relationship between variables. It can also be a methodical approach to altering in order to measure the cause-and-effect relationship between the process inputs and outputs as well as the random variability of the process while requiring the least number of runs. Experimentation is a very vital aspect of scientific study, which can be developed using computer software's like design expert and Minitab. For better polynomial approximation an experimental design is used to collect the data. There are different types of experimental designs which includes central composite circumscribed, central composite face centred, full factorial, and Latin hyper cube designs.

2.3 Identification of range of input parameters

Welding current, welding voltage, wire diameter, and wire feed speed are the main factors that were taken into account in this study. Table 1 displays the variety of process variables gleaned from the literature.

2.4. Scanning electron microscope (SEM)

In order to identify any phase changes at the cleaned surfaces, SEM was utilized to examine the laser-cleaned surfaces in comparison with a reference surface. As seen in Figure 1, a Hitachi High Technologies S-3400N Type I, 0.1-30 kV scanning electron microscope was employed.

Table 1: Process parameters and their levels

Factors	Unit	Symbol	Low (-1)	High (+1)
Welding Current	Ampere	I	180	240
Welding Voltage	Volts	V	18	24
Wire diameter	Mn	WD	1.2	3.0
Wire feed speed	Mm/min	WFS	10	50

Figure 2: Hitachi High Technologies S-3400N SEM (Hitachi S-3400N)

2.5 Method of Data Collection

Using design expert software, the center composite design matrix was created, yielding 20 experimental runs. The experimental matrix is made up of the input and output parameters, and the responses noted for the weld samples were utilized as the data. The data matrix is determined by the number of input parameters, which is provided by the equation 2n + 2n + k, where k is the quantity of center points, 2n is the quantity of axial points, and 2n is the quantity of factorial points. The data obtained were analyzed using the following techniques.

2.6 Method of Data Analysis

2.6.1 Response Surface Methodology (RSM)

RSM is one of the optimization methodologies that is currently in widespread use to describe the performance of the welding process and choose the appropriate response. RSM is a collection of mathematical and statistical methods that are useful for modeling and forecasting the interest response, which is influenced by a number of input variables, in order to optimize the response. The optimal value for a given function in terms of the process input parameters could either be minimal or maximum.

Table 2: Analysis of Variance Components

Variation Source	Degree of Freedom Df	Sum of Squares SS	Mean Square MS	Fisher Ratio F-value
Error of residuals	n-2	$SSE = \sum_{i=1}^{c}\sum_{j=1}^{ni}(y_{ij} - \hat{y}_{ij})^2$	$MSE = \frac{SSE}{n-2}$	
Regression	1	$SSR = \sum_{i=1}^{c}\sum_{j=1}^{ni}(\hat{y}_{ij} - \bar{y})^2$	$MSR = \frac{SSR}{1}$	$F = \frac{MSR}{MSE}$
Lack of fit	C -2	$SSLF_i = \sum_{i=1}^{c}\sum_{j=1}^{ni}(\bar{y}_{ij} - \hat{y}_{ij})^2$	$MSLF = \frac{SSLF}{c-2}$	$F^* = \frac{MSLF}{MSPE}$
Total	n-1	$SSTD = \sum_{i=1}^{c}\sum_{j=1}^{ni}(y_{ij} - \bar{y}_{ij})^2$	-	-

2.6.2 Artificial Neural Network

A massively parallel distributed processor called a neural network that is naturally inclined to store experimental information and make it accessible for application. It is used as a data mining tool to identify unknown patterns in datasets. In two ways, it resembles the brain. R-input to an elementary neuron is weighted with the appropriate w. The input to the transfer function f is made up of the bias added to the weighted inputs. In order to generate their output, neurons can use any differentiable transfer function f. The transfer function logsig of a log-sigmoid is frequently used in multilayer networks. The function logsig generates outputs between 0 and 1 as the neuron's net input changes from a negative value to a positive infinity. The

tan-sigmoid transfer function, or tansig, in multilayer networks provides an alternative. Sigmoid output neurons are widely used, although linear output neurons are when it comes to pattern recognition problems. The artificial neural network is a data mining tool, which uses the theory of the human brain and the neurone communication technique that has been programmed into a software. It is a predictive tool analyses a data by the following process: training, learning validating and testing. The neural network flow diagram is presented in figure 2.

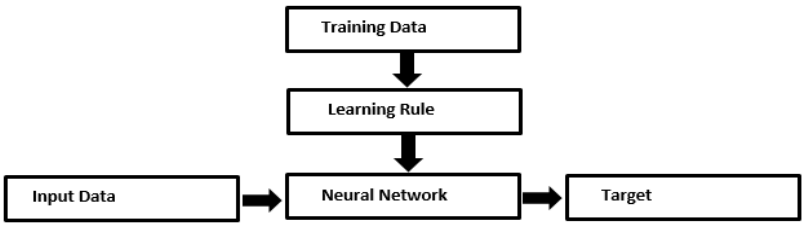

Figure 2: Neural network flow diagram

The link between the input, hidden neurons, and output is built using the optimal number of hidden neurons, as shown by the simple neural network diagram in figure 3.

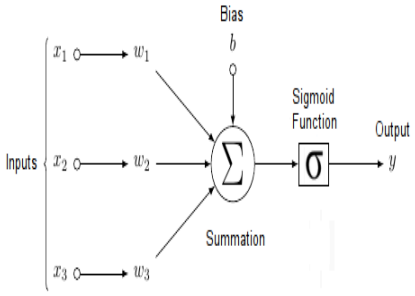

Figure 3: Simple Neural Network Diagram

X_1, X_2 and X_3 are the signals entering the nodes which can also be taken as the sample parameters, these signals enter the node. W1, W2, and W3 are the matching weights of the signals, and 'b' is referred to as bias, which is connected to the storage of information. Y is the Target or Output. Weights and bias are the two ways that information is stored in neural networks.

3. RESULTS

Both the response surface methodology (RSM) and the artificial neural network (ANN) were utilized in this investigation to analyze the data gathered from the trials conducted.

3.1 Modeling and Optimization using Response Surface Methodology (RSM)

The second order effects of non-linear relationships are included in the Response Surface Model, a modification on simple linear regression. The optimization model's goal is to increase the electrode density. Identifying the optimal value for each input variable (current (Amp), voltage (V) wire

diameter and wire feed speed) is the process's final answer that will give us the best weld electrode density. For the purpose of producing experimental data for optimization:

(i) An experiment's statistical design was carried out utilizing the central composite design method (CCD). A statistical tool was used to carry out the design and optimization. It was decided to use Design Expert 7.01.

(ii) 30 experimental runs were created used a matrix for experimental design with sixteen factorial points (2n), eight axial points (2n), and six center points (k).

The sequential model sum of squares for the electrode density response was calculated to confirm that the quadratic model was appropriate for evaluating the experimental data, and the results are shown in Table 3.

Table 3: Sequential model sum of square for electrode density

Source	Sum of Squares	df	Mean Square	F Value	p-value Prob > F	
Mean vs Total	1.325E+009	1	1.325E+009			
Linear vs Mean	1.026E+005	4	25639.42	6.80	0.0008	
2FI vs Linear	34197.42	6	5699.57	1.80	0.1519	
Quadratic vs 2FI	54348.67	4	13587.17	36.00	< 0.0001	Suggested
Cubic vs Quadratic	4561.04	8	570.13	3.63	0.0533	Aliased
Residual	1099.95	7	157.14			
Total	1.325E+009	30	4.416E+007			

The sequential model sum of squares table illustrates how the model fit becomes better as more terms are added. As the best fit, the highest order polynomial with significant additional terms and no aliasing was chosen based on the estimated sequential model sum of squares.

The lack of fit test was calculated for each response to determine how well the quadratic model accounts for the underlying variation in the experimental data. Prediction cannot be made using a model with a considerable lack of fit. Table 4 displays the findings of the computed lack of fit for the electrode density factor.

The quadratic model's applicability was determined by the goodness of fit statistics presented in table 5 based on its ability to maximize electrode density.

Any model's acceptability must first be verified by the results of an acceptable statistical analysis. Figures 4 and 5 display the residuals probability plot and the residuals against expected for electrode density, respectively, to diagnose the statistical features of the response surface model.

For electrode density, which is depicted in figure 8, the projected values are displayed against the actual values in order to identify a value or set of values that the model has difficulty identifying. Figures 6 and 7 show the generated cook's distance for the electrode density.

Figures 8 and 9 provide 3D surface plots for the electrode density to examine the effects of many input factors.

Table 4: Lack of fit test for electrode density

Source	Sum of Squares	Df	Mean Square	F Value	p-value Prob > F	
Linear	93601.38	20	4680.07	38.63	0.0004	
2FI	59403.96	14	4243.14	35.03	0.0005	
Quadratic	5055.29	10	505.53	4.17	0.0642	Suggested
Cubic	494.25	2	247.13	2.04	0.2250	Aliased
Pure Error	605.70	5	121.14			

Table 5: Goodness of fit statistics for electrode density

Std. Dev.	19.43	**R-Squared**	0.9712
Mean	6644.62	**Adj R-Squared**	0.9444
C.V. %	0.29	**Pred R-Squared**	0.8476
PRESS	29990.67	**Adeq Precision**	28.014

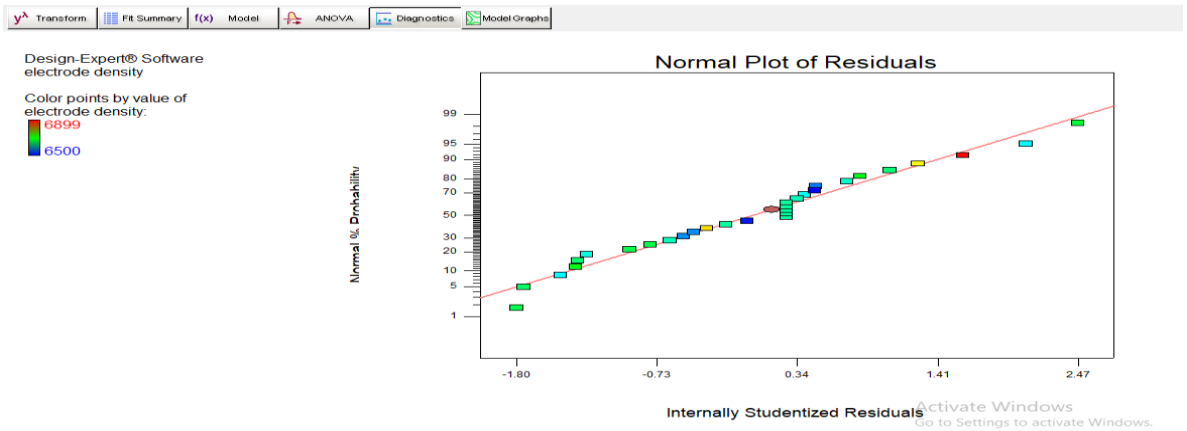

Figure 4: probability plot of residuals for electrode density

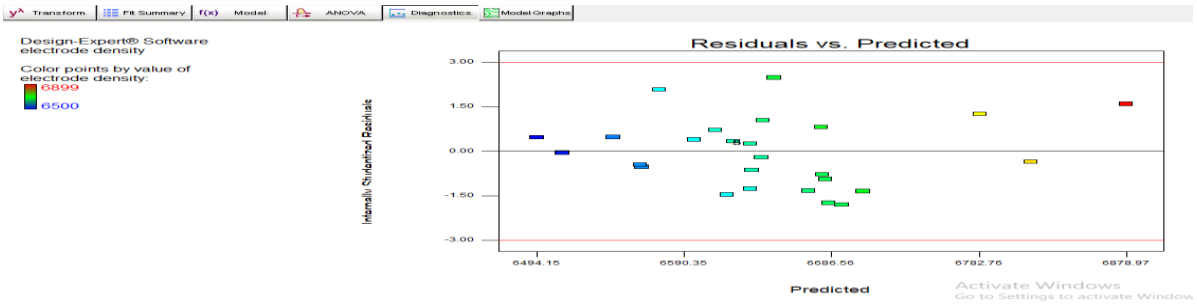

Figure 5: plot of residuals against predicted for electrode density

*Corresponding author, e-mail:author@fupre.edu.ng
DIO

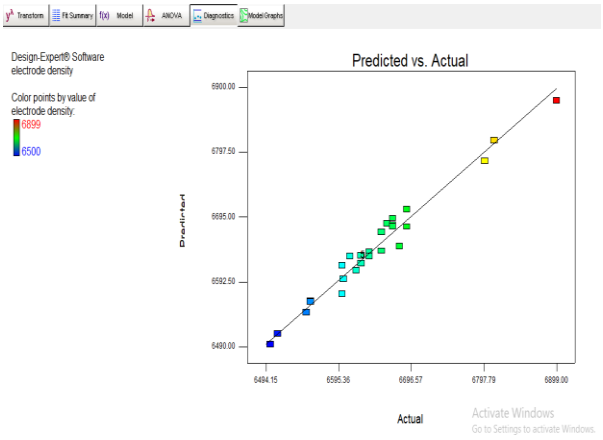

Figure 6: Plot of Predicted Vs Actual for electrode density

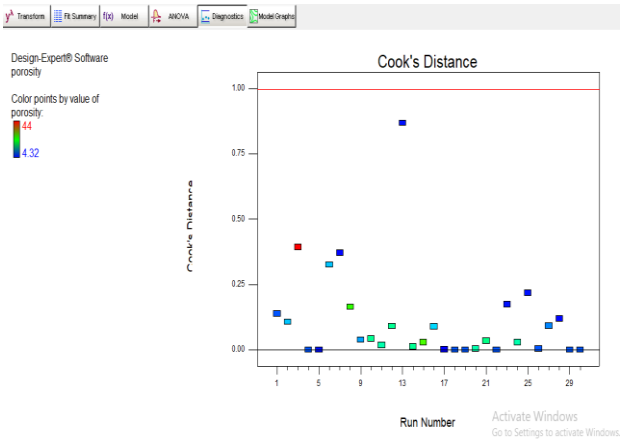

Figure 7: The generated cook's distance for the electrode density

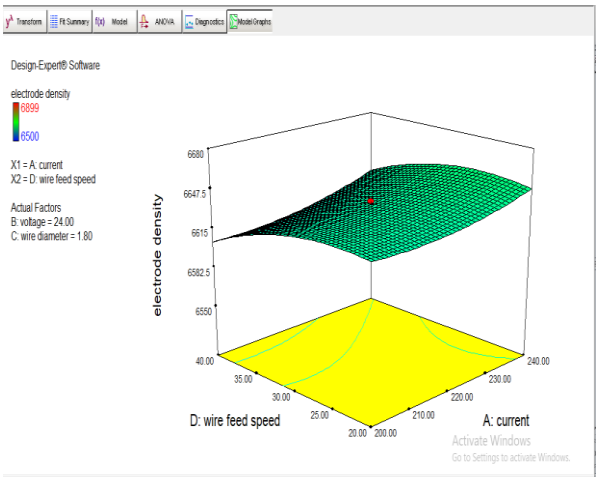

Figure 8: Effect of current and voltage on electrode density

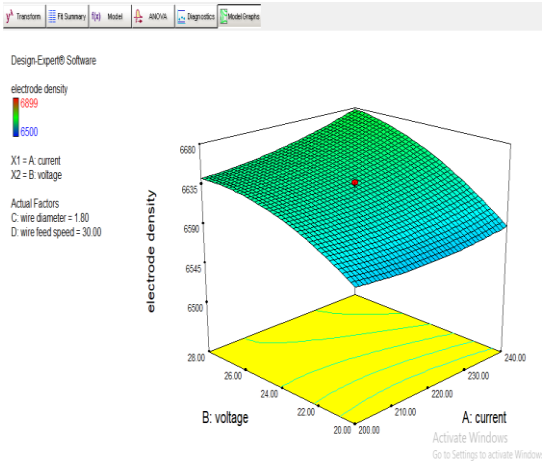

Figure 9: Effect of wire feed speed and current on electrode density

3.2 Modeling and Optimization using the Artificial Neural Network (ANN)

The input and output interphase for the electrode density factor response is a 4 x 30 matrix, such that the input parameters (current, voltage wire diameter and wire feed speed) and targetted response (electrode density) were selected as were inputed into ANN. It is recommended that a set of data be set aside for validation and testing. Data obtained from this research were divided into three parts with 70% of the experimental sample data used for training, 15% used for validation, whereas the final 15% was tested for the neural network model. This resulted in 20 samples

of the entire population used for training validation and testing. Figure 10 depicts the network architecture of the ANN, which comprises four inputs, ten neurons in the hidden layer, and one neuron in the output layer.

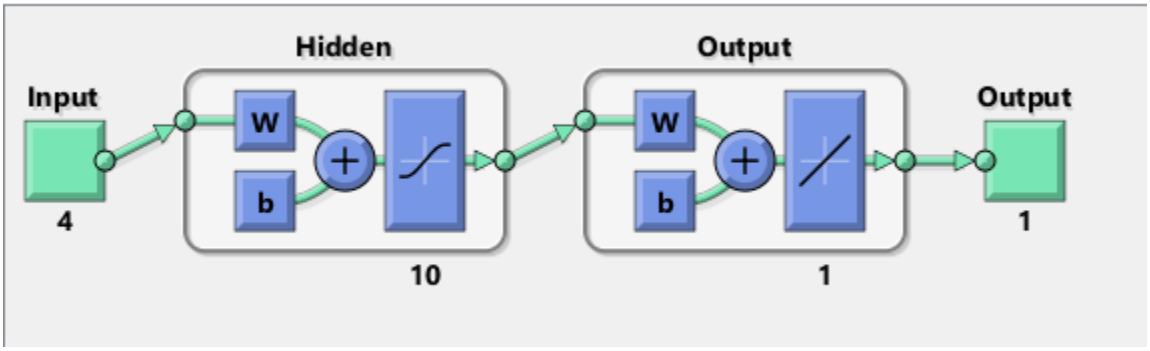

Figure 10. Artificial neural network architecture for predicting the electrode density.

The Training interphase: from the result summary, it was noticed that the training of the network model provided a correlation having 90.6% with a mean square error of 8.98E-3. The validation of the network model produced a correlation of 91.3% with a mean square error of 3.57E-2. The network model's testing yielded an 80.9% correlation with a mean square error of 1.96E-2. Levenberg-Marquardt was selected as the training algorithm, Mean Squared Error as the performance algorithm, and the data division strategy was set to random (dividerand). The performance plot, plotted to check for network learning is shown in figure 11, while the gradient function plot to show how much errors produced during prediction is shown in figure 12.

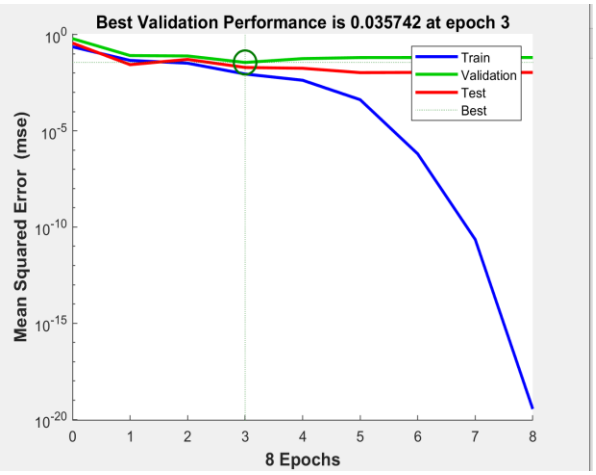

Figure 11: Performance curve for trained network to predicting electrode density responses

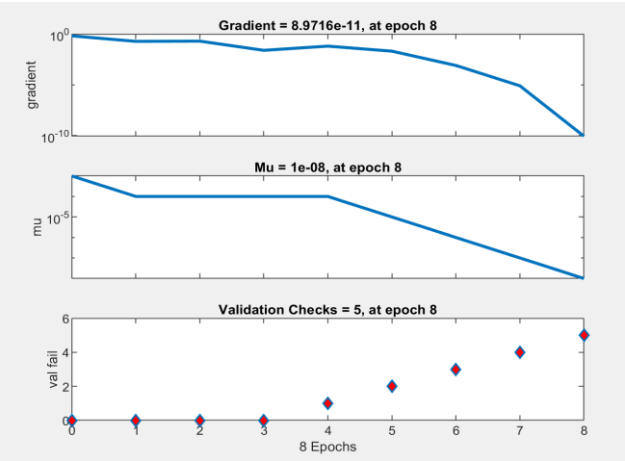

Figure 12: Neural network gradient plot for predicting electrode density responses

*Corresponding author, e-mail:author@fupre.edu.ng
DIO

In figure 13, the best prediction for the electrode density responses was achieved at epoch 3, although, a total of 8 epochs were used in the iteration process. A regression plot is produced to check for the coefficient of correlation and the closeness between the network output and the experimental data. Figure 13 displays the regression plot illustrating the training, validation, and testing of the network output.

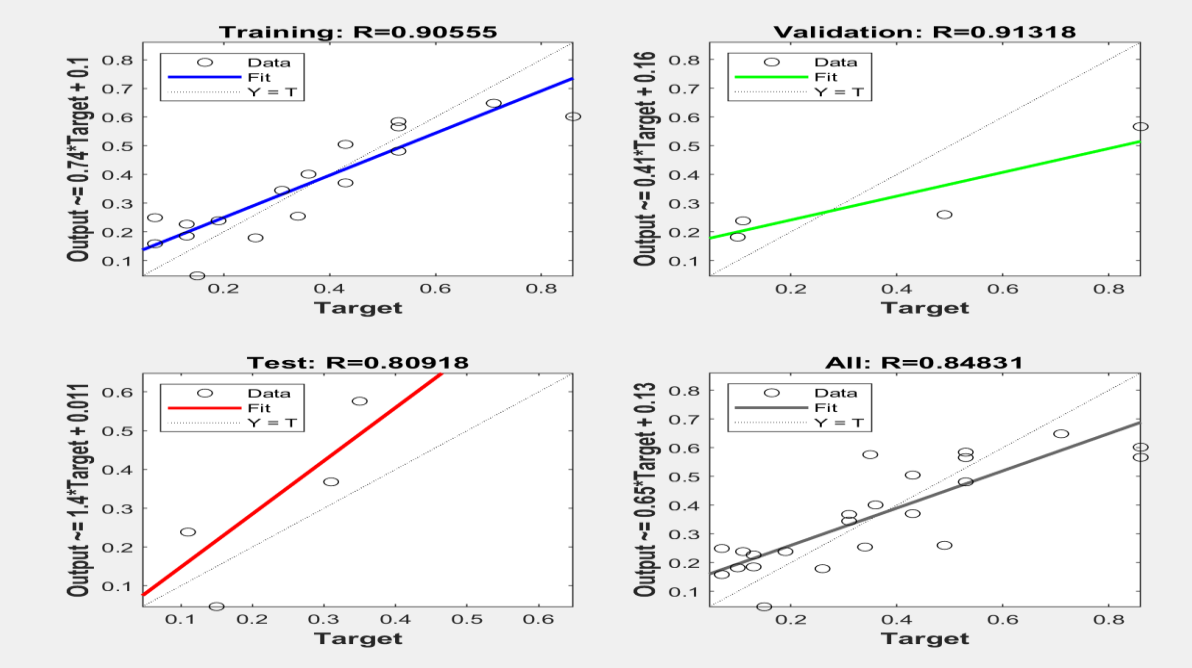

Figure 13: Regression plot of training, validation and testing for electrode density responses

With a correlation coefficient (R) of more than 80%, Figure 13 shows the training, validation, and testing plot and denotes a reliable prediction for the electrode density. The dotted diagonal line on each plot indicates the line of best fit which indicate a perfect prediction and a correlation of 1.

3.3 Comparison of the Experimental values and ANN predicted values

A time series plot can help to appreciate the graphical difference between the experimental result and the network output which is shown in figure 14 while a fitted plot for the artificial network output was done to ilustrate the correlation between the experimental and the model developed, this is shown in figure 15

*Corresponding author, e-mail:author@fupre.edu.ng
DIO

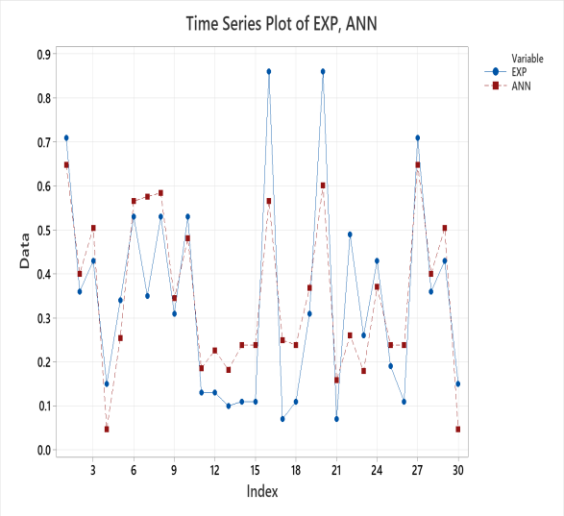

Figure 14: A time series plot of experimental values and network output for electrode density

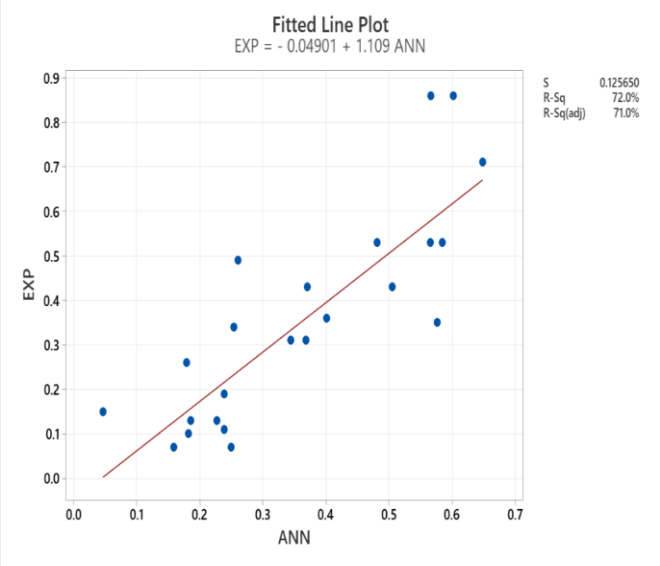

Figure 15: Fitted line plot for electrode density

Equation (1) provides the regression equation for the electrode density response between the experimental and expected values.

EXP = - 0.04901 + 1.109 ANN

(1)

The model summary statistics for the network shows the strength of the network output. The result is shown in table 7.

Table 7: ANN Model Summary for electrode density

S	R-sq	R-sq(adj)
0.125650	71.96%	70.96%

1

The analysis of variance for the network output to check for the significance of the network is shown in table 8.

Table 8: ANN Analysis of Variance for weld strength factor

Source	DF	SS	MS	F	P
Regression	1	1.13461	1.13461	71.87	0.000
Error	28	0.44206	0.01579		
Total	29	1.57667			

3.4 Discussion

The two expert methods, namely, Response Surface methodology (RSM), and the artificial neural network (ANN) have been employed to explain the existing link between welding process input parameters such as current, voltage, wire diameter, and wire feed speed in correspondence with the electrode density. The RSM and the ANN methods were utilized in predicting and optimising the weld response. The RSM results showed the second order polynomial model best explains the behavior of the experimental data. The similarities of the process parameters and the electrode density is quadratic, and shows a strong correlation between the voltage, wire diameter and electrode density with a p value < 0.00001. The variance inflation factor (VIF) was 1.00 which shows that the model is significant because a (VIF) greater than 10.00 is a cause for alarm. The goodness of fit statistics provided an R2 of 0.9712 for the coefficient of determination, which may be used to

*Corresponding author, e-mail:author@fupre.edu.ng
DIO

verify the importance and suitability of the model based on its capacity to forecast electrode density. The noise to signal ratio for the model is 28.014, which is higher than 4 and suggests a sufficient signal. Numerical optimization was eventually achieved. With a desirability value of 0.939, Design Expert 7.01 software chose this solution as the best one. The artificial neural networks were also used to predict the electrode density. The input data are randomly divided into three sets. 70% are used to train the network, 15% are used to validate the network performance and 15% are used for the test. For training, the Levenberg Marquardt algorithm was utilized. For the training interphase the network provided a correlation value of 90.5% with a mean square error of 8.97e-3. The validation of the network model produced a correlation value of 91.3% with a mean square error of 3.574e-2. The testing of the network model produced a correlation of 80.9% with mean square error 1.963e-5. The performance plot and the correlation plot showed that the network learnt accurately and can be used to predict the target responses.

4. CONCLUSION

The strength and quality of a weld are determined by minimizing faults and enhancing responses that improve weld quality, the more electrodes in a weld structure, the better. In this study, a key output parameter was predicted and optimized using the response surface methodology (RSM) and the artificial neural network (ANN) model. From the results obtained, it is seen that (i) the ANOVA result showed that the lower the current and wire diameter the higher the electrode density of the weld and (ii) the optimal solution of the RSM model is preferred as it is able to predict maximized electrode density. Hence, the response surface methodology provided better optimal solution. The application of expert systems, such as artificial neural network models and response surface technique, increased the quality of tungsten inert gas welding. This study optimized electrode density as a welding response, thus, the optimal solution will help to produce welds with better strength, reliability and accuracy by testing and validating the models produced.

Declaration of Competing Interest

The authors declare that they have no known competing interests.

References

Aumm graphixphoto, Shutterstock https://waterwelders.com

Azadi M. and Kolahan F., (2020) 'Optimization of A-TIG welding process using simulated annealing algorithm,' Journal of Advanced Manufacturing Systems, 19 (4), 869–891.

Bhadeshia, H.; Honeycombe, R. (2017) Chapter 12-Stainless Steel BTSteels, Microstructure and Properties (Fourth edition), Butterworth-Heinemann, 343-376.

Dipali P., Amarish B. and Nilesh G. (2021) A novel perception toward welding of stainless steel by activated TIG welding: a review, Materials and Manufacturing Processes, 36(8), 877-903.

Hall, J and Fekete, J. (2017) 'Steels for auto bodies: A general overview Automotive Steels', Woodhead Publishing, 19-45.

Hitachi S-3400N. elsevierpure.com

Magudeeswaran G., Nair S., L. Sundar, and N. Harikannan, (2014) 'Optimization of process parameters of the activated tungsten inert gas welding for aspect ratio of UNS S32205 duplex stainless

steel welds', Defence technology, 10 (3), 251-260

Meneses, L., Silva, A. and Alfaro, S. (2019) 'Modeling and simulation of the metal transfer on GMAW-S process. J Braz. Soc. Mech. Sci. Eng. **41**, 550.

Pamnani R., Vasudevan M., Vasantharaja P., and Jayakumar T., (2017) 'Optimization of A-GTAW welding parameters for naval steel (DMR 249 A) by design of experiments approach'. Proceedings of the Institution of Mechanical Engineers-Part L: Journal of Materials: Design and Applications, 231 (3), 320-331.

Pongsak14, Shutterstock, https://waterwelders.com

Ragavendran M., Chandrasekhar N., Ravikumar R., Saxena R., Vasudevan M., and Bhaduri A. (2017) 'Optimization of hybrid laser–TIG welding of 316LN steel using response surface methodology (RSM)', Optics and Lasers in Engineering, 94, 27-36.

Sarkar P. and Kakoty S., (2021) 'Pareto optimization of TIG welding process for joining the bell metal'. Materials and Manufacturing Processes', 37 (8), 956-964.

Sathish T., Tharmalingam S., Mohanavel V. (2021) 'Weldability investigation and optimization of process variables for TIG-welded aluminium alloy (AA 8006)', Advances in Materials Science and Engineering, 1-17.

Singh P., Kumar S., Patel D., and Prasad S. (2017) 'Optimization of vibratory welding process parameters using response surface methodology', Journal of Mechanical Science and Technology, 31 (5), 2487–2495.

Sivachidambaram P. and Balachandar K. (2015), 'Optimization of pulsed current TIG welding parameters on al-sic metal matrix composite-An empirical approach', Indian Journal of Science and Technology, 8 (23), 1.

Sunilkumar, D., Muthukumaran, S., Vasudevan, M., Reddy, M. (2020) 'Effect of friction stir and activated-GTA welding processes on the 9Cr–1Mo steel to 316LN stainless steel dissimilar weld joints'. Sci. Technol. Weld. Join., 25(4), 311–319.

Vasantharaja P and Vasudevan M. (2018), 'Optimization of A-TIG welding process parameters for RAFM steel using response surface methodology', Proceedings of the Institution of Mechanical Engineers-Part L: Journal of Materials: Design and Applications, 232 (2), 121–136.

Vidyarthy R., Dwivedi D., and Muthukumaran V. (2018), 'Optimization of A-TIG process parameters using response surface methodology', Materials and Manufacturing Processes, 33 (7), 709–717.